Analysis of Asymmetrical Multilayer Ferrite-Loaded Finlines by the Extended Spectral Domain Approach

Z. Fan and Steve R. Pennock, *Member, IEEE*

Abstract—**The spectral domain approach is extended to analyze the nonreciprocal propagation characteristics of asymmetrical multilayer finlines containing magnetized ferrites. This extended method offers several advantages. It can be applied to nonuniform cross-section geometries, uses only one set of basis functions, and the dyadic Green's function is efficiently derived by a recursive algorithm. Fast convergence is obtained and the accuracy of the method is verified by comparison with available computed and measured data. In comparison with symmetrical structures, the additional design degree of freedom of the asymmetry can be used to obtain wider bandwidth and higher nonreciprocity. Of the various structures considered, a four-layer dual ferrite (DF) structure is seen to be the best choice for realization of nonreciprocal phase shifters with widest bandwidth.**

I. Introduction

FINLINES have been extensively investigated for use in microwave and millimeter wave integrated circuits. A wide variety of finline circuit components have been developed including nonreciprocal ferrite devices such as nonreciprocal phase shifters, isolators, and circulators [1], [2]. Several methods, including field expansion, mode-matching, network analysis and the spectral domain approach as in [2]–[6], have been reported for the analysis of nonreciprocal propagation characteristics of single or multilayer ferrite-loaded finlines. However, all these techniques treated only symmetrical structures. The effects found in an asymmetrical structure, such as is shown in Fig. 1 where $a \neq a_0$, have not been studied to date. Furthermore, only single-ferrite finline structures have been considered and only their differential phase shift was discussed.

Recently, the asymmetrical finline has been proposed [7] for space applications. Several advantages over conventional, symmetrical finlines are apparent, including ease of substrate and device mounting, wider single-mode bandwidth, and the additional design degree of freedom offered by the asymmetrical fin shielding. Devices such as filters and mixers have been developed in the asymmetrical finline form, and the propagation characteristics of the asymmetrical finlines with a dielectric substrate have been analyzed using the spectral domain method [7], [8]. To realize nonreciprocal components at millimeter wave frequencies, ferrite layers need to be inserted into a multilayer configuration. However, so far no efforts have been devoted to the analysis of asymmetrical multilayer finlines with magnetized ferrites.

Manuscript received August 8, 1994; revised December 18, 1995.

The authors are with the School of Electronic and Electrical Engineering, University of Bath, Bath BA2 7AY, UK.

Publisher Item Identifier S 0018-9480(96)02349-6.

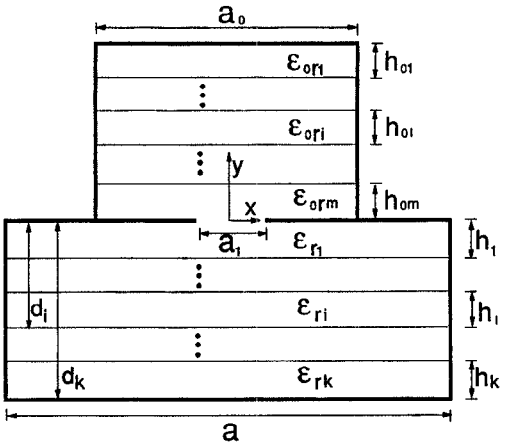

Fig. 1. Cross section of an asymmetrical multilayer finline where any layer can be dielectric or ferrite and coordinate system used in the analysis.

The purpose of this paper is to extend the spectral domain approach so that asymmetrical multilayer finlines containing magnetized ferrites can be analyzed. We present a recursive algorithm to derive the Fourier transformed dyadic Green's function for the different regions of the structures. Galerkin's procedure is applied to obtain solutions, and our data are seen to compare favorably with published data. The advantages of asymmetrical finlines are demonstrated, and the effects obtainable in various multilayer configurations on the nonreciprocity and bandwidth are investigated.

II. Field Representation by Fourier Transforms

Fig. 1 illustrates the cross section of an asymmetrical multilayer finline and the coordinate system to be used in the analysis. This structure consists of asymmetrically shielded metal fins sandwiched between two multilayer substrates, where any layer can be a magnetized ferrite or a dielectric. The assumed time and z dependence $\exp j(wt - \beta z)$ is for all the field and current quantities, and omitted in the following analysis for the sake of brevity.

Discrete Fourier transforms are used to represent the field components in this structure, for instance

$$H_x(x,y) = \frac{1}{a} \sum_{n=-\infty}^{\infty} \tilde{H}_x(\alpha, y) e^{-j\alpha x}. \tag{1}$$

To satisfy the electric field boundary conditions at the sidewalls of the lower ($y < 0$) and upper ($y > 0$) regions, different transform variables, $\alpha = \alpha_n$ and $\alpha = \alpha_{0n}$, respectively, have

to be chosen for these regions. In the lower region ($y<0$) the values of α_n are equal to $2n\pi/a$ for the E_z odd modes and to $(2n+1)\pi/a$ for the E_z even modes with $n=0,\pm1,\pm2,\cdots$. For the upper region ($y>0$)a is replaced by a_0.

If the ith layer in the lower region is a lossless ferrite that is magnetized to saturation in the x direction, it is characterized by a scalar relative permittivity ε_{ri} and a permeability tensor [5]

$$\hat{\mu}=\mu_0\begin{bmatrix}1 & 0 & 0\\ 0 & \mu_r & -j\kappa\\ 0 & j\kappa & \mu_r\end{bmatrix} \tag{2}$$

where μ_0 is the free space permeability. μ_r and κ are dependent on the angular frequency, the applied dc magnetic field H_0 and the saturation magnetization of the ferrite M_0.

From Maxwell's curl equations we obtain coupled wave equations for the x-directed electric and magnetic field components in the Fourier transform domain

$$\frac{\partial^2\tilde{H}_x}{\partial y^2}-\gamma_h^2\tilde{H}_x=\eta_h\tilde{E}_x \tag{3}$$

$$\frac{\partial^2\tilde{E}_x}{\partial y^2}-\gamma_e^2\tilde{E}_x=\eta_e\tilde{H}_x \tag{4}$$

where $\gamma_h^2,\eta_h,\gamma_e^2$, and η_e are given in [5].

Other Fourier transformed field components can be expressed in terms of $\tilde{H}_x$ and $\tilde{E}_x$ and their derivatives. Multiplying (3) by η_e, operating $\partial^2/\partial y^2-\gamma_h^2$ on (4) and adding results in the following fourth-order differential equation for $\tilde{E}_x$

$$\left(\frac{\partial^2}{\partial y^2}-\gamma_+^2\right)\left(\frac{\partial^2}{\partial y^2}-\gamma_-^2\right)\tilde{E}_x=0 \tag{5}$$

where

$$\gamma_\pm^2=0.5\left(\gamma_h^2+\gamma_e^2\pm\sqrt{(\gamma_h^2-\gamma_e^2)^2+4\eta_h\eta_e}\right).$$

The solution to the equation can be expressed in terms of linear combinations of sinh and cosh functions with two different transverse wavenumbers in the y direction and contains the four unknown modal amplitudes. The coefficients are determined by introducing the tangential electric field components on the upper and lower surfaces of the layer. Then the relationship between the tangential magnetic and electric field components on the surfaces i and $j=i-1$ can be obtained in the following matrix form

$$\begin{bmatrix}\tilde{H}_z(\alpha_n,d_j)\\ -\tilde{H}_x(\alpha_n,d_j)\\ \tilde{H}_z(\alpha_n,d_i)\\ -\tilde{H}_x(\alpha_n,d_i)\end{bmatrix}=\begin{bmatrix}P_i & S_i\\ R_i & T_i\end{bmatrix}\begin{bmatrix}\tilde{E}_x(\alpha_n,d_j)\\ \tilde{E}_z(\alpha_n,d_j)\\ \tilde{E}_x(\alpha_n,d_i)\\ \tilde{E}_z(\alpha_n,d_i)\end{bmatrix} \tag{6}$$

where the 2×2 submatrices $[P_i],[R_i],[S_i]$, and $[T_i]$ depend only on the electromagnetic properties and the thickness of the ith layer. These are given in the Appendix and will be used to derive the recursive algorithm in the following section. If the ith layer of the lower region is a dielectric ($\mu_r=1$ and $\kappa=0$), and characterized by scalar relative permittivity ε_{ri} and scalar permeability μ_0, the wave equations for $\tilde{H}_x$ and $\tilde{E}_x$ will be uncoupled. There then exist TE-to-y and TM-to-y modes, whose solutions for field components are well known [9]. In this case, the elements of the submatrices in (6) can be easily obtained, and these are also given in the Appendix.

III. Recursive Derivation of the Green's Function

To derive the integral equations for the tangential electric field components on the aperture plane ($y=0$), Green's functions for both regions have to be obtained first. There are many techniques for deriving the multilayer Green's functions. These include the spectral domain immitance approach [10], the mixed spectral domain approach [8], the matrix method [11], and the equivalent boundary method [12]. Most of them assume isotropic media. Others can treat anisotropic media, but cannot be applied to structures with nonuniform cross sections. We now present a new recursive algorithm to derive the Green's functions for the multilayer anisotropic structure with a nonuniform cross section as shown in Fig. 1. First, we consider the lower region ($y<0$). The relationship between the tangential magnetic and electric field components at $y=0^-$ and the lower surface of the jth layer can be expressed in the following matrix

$$\begin{bmatrix}\tilde{H}_z(\alpha_n,0^-)\\ -\tilde{H}_x(\alpha_n,0^-)\\ \tilde{H}_z(\alpha_n,d_j)\\ -\tilde{H}_x(\alpha_n,d_j)\end{bmatrix}=\begin{bmatrix}P^{(0,j)} & S^{(0,j)}\\ R^{(0,j)} & T^{(0,j)}\end{bmatrix}\begin{bmatrix}\tilde{E}_x(\alpha_n,0^-)\\ \tilde{E}_z(\alpha_n,0^-)\\ \tilde{E}_x(\alpha_n,d_j)\\ \tilde{E}_z(\alpha_n,d_j)\end{bmatrix}. \tag{7}$$

It should be noted that in (6) and (7) the components $\tilde{H}_z,\tilde{H}_x,\tilde{E}_z$, and $\tilde{E}_x$ are continuous at the interface between the jth and ith layers. Similarly, we can establish the following relationship between the tangential magnetic and electric field components at $y=0^-$ and the lower surface of the ith layer

$$\begin{bmatrix}\tilde{H}_z(\alpha_n,0^-)\\ -\tilde{H}_x(\alpha_n,0^-)\\ \tilde{H}_z(\alpha_n,d_i)\\ -\tilde{H}_x(\alpha_n,d_i)\end{bmatrix}=\begin{bmatrix}P^{(0,i)} & S^{(0,i)}\\ R^{(0,i)} & T^{(0,i)}\end{bmatrix}\begin{bmatrix}\tilde{E}_x(\alpha_n,0^-)\\ \tilde{E}_z(\alpha_n,0^-)\\ \tilde{E}_x(\alpha_n,d_i)\\ \tilde{E}_z(\alpha_n,d_i)\end{bmatrix}. \tag{8}$$

Combining (6) with (7), the submatrices in (8) can be derived in terms of the submatrices in (6) and (7). This results in the following recursive equations

$$[P^{(0,i)}]=[P^{(0,j)}]+[S^{(0,j)}][V][R^{(0,j)}] \tag{9}$$

$$[R^{(0,i)}]=[R_i][V][R^{(0,j)}] \tag{10}$$

$$[S^{(0,i)}]=-[S^{(0,j)}][V][S_i] \tag{11}$$

$$[T^{(0,i)}]=-[R_i][V][S_i]+[T_i] \tag{12}$$

where $i=2,3,\cdots,k$ (k is the number of layers in the lower region) and

$$[V]=[U]^{-1},\quad [U]=[P_i]-[T^{(0,j)}]. \tag{13}$$

For $i=1$, we have

$$\begin{bmatrix}P^{(0,1)} & S^{(0,1)}\\ R^{(0,1)} & T^{(0,1)}\end{bmatrix}=\begin{bmatrix}P_1 & S_1\\ R_1 & T_1\end{bmatrix}. \tag{14}$$

The tangential electric field components must be zero at the bottom conducting plane of the lower region, and using (8)

with $i = \mathrm{k}$, the magnetic field Green's function for the lower region can be obtained as follows:

$$\begin{bmatrix} \tilde{H}_z(\alpha_n, 0^-) \\ -\tilde{H}_x(\alpha_n, 0^-) \end{bmatrix} = [Y(\alpha_n)] \begin{bmatrix} \tilde{E}_x(\alpha_n, 0^-) \\ \tilde{E}_z(\alpha_n, 0^-) \end{bmatrix} \quad (15)$$

where $[Y] = [P^{(0,k)}]$. Similarly the magnetic field Green's function for the upper region, $[Y^0(\alpha_{0n})]$, can be also obtained.

Employing the boundary conditions for the tangential electric and magnetic field components at the aperture plane we obtain the following integral equations for the tangential electric field components at the aperture $|x| < a_1/2$

$$\frac{1}{a_0} \sum_{n=-\infty}^{\infty} [Y^0(\alpha_{0n})] \begin{bmatrix} \tilde{E}_x^b(\alpha_{0n}) \\ \tilde{E}_z^b(\alpha_{0n}) \end{bmatrix} e^{-j\alpha_{0n}x} + \frac{1}{a} \sum_{n=-\infty}^{\infty} [Y(\alpha_n)] \begin{bmatrix} \tilde{E}_x^b(\alpha_n) \\ \tilde{E}_z^b(\alpha_n) \end{bmatrix} e^{-j\alpha_n x} = 0 \quad (16)$$

where $\tilde{E}_x^b$ and $\tilde{E}_z^b$ are the Fourier transforms of the x and z electric field components at the aperture ($y = 0$).

IV. Application of Galerkin's Method

Galerkin's procedure is applied [13] to the integral equations (16), resulting in a homogeneous matrix equation for the unknown expansion coefficients

$$\begin{bmatrix} K_{im}(x,x) & K_{im}(x,z) \\ K_{im}(z,x) & K_{im}(z,z) \end{bmatrix} \begin{bmatrix} C_{xm} \\ C_{zm} \end{bmatrix} = [0]. \quad (17)$$

The elements of matrix $[K]$ are given by

$$K_{im}(p,r) = \frac{1}{a_0} \sum_{n=-\infty}^{\infty} \tilde{E}_{pi}^b(-\alpha_{0n}) Y_{pr}^0(\alpha_{0n}) \tilde{E}_{rm}^b(\alpha_{0n}) + \frac{1}{a} \sum_{n=-\infty}^{\infty} \tilde{E}_{pi}^b(-\alpha_n) Y_{pr}(\alpha_n) \tilde{E}_{rm}^b(\alpha_n) \quad (18)$$

where p and r denote x or z and

$$\tilde{E}_{pm}^b(\alpha_n) = \int_{-\frac{a_1}{2}}^{\frac{a_1}{2}} E_{pm}^b(x) e^{j\alpha_n x}\, dx. \quad (19)$$

For (17) to yield a nontrivial solution, the determinant of $[K]$ must to zero. This results in a determinantal equation for the propagation constants in the positive and negative z directions, β_+ and β_-, respectively.

To evaluate elements of the matrix $[K]$ the Fourier transforms of basis functions in (19) need to be obtained. The basis functions should contain the singular behavior of the electric field components at the edges of metal fins in order to achieve good numerical efficiency and accuracy for the determinantal equation. The two tangential electric field components at the aperture satisfy different edge conditions, and in the conventional spectral domain approach, two sets of basis functions are used. By integrating (19) by parts [13], it is possible to describe the problem in terms of $\partial E_z^b(x)/\partial x$ and $E_x^b(x)$. These have the same $r^{-0.5}$ singularity at the fin edges. Chebyshev polynomials, $T_m(x)$, are used for the basis

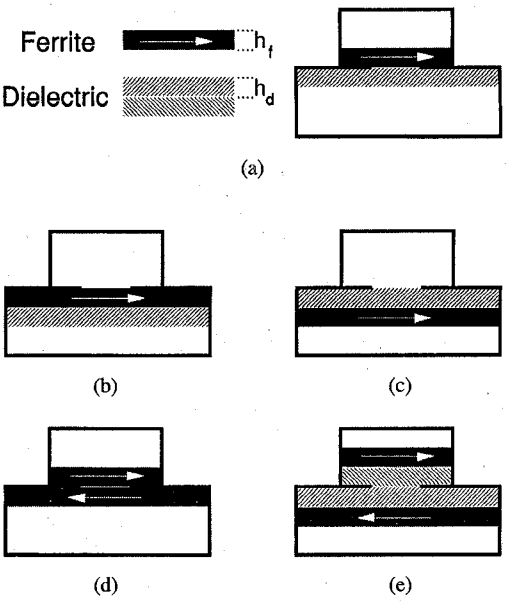

Fig. 2. Cross section of an asymmetrical finline loaded with (a) sandwich ferrite-dielectric (SWFD), (b) double layer ferrite-dielectric (DLFD), (c) double layer dielectric-ferrite (DLDF), (d) dual-ferrite (DF), and (e) dual-ferrite-dielectric (DFD). The relative dielectric constants of the ferrite and dielectric regions are ϵ_{rf} and ϵ_{rd}, respectively. The heights of the air layers in the upper and lower regions are h_0 and h_1, respectively.

functions as they are orthogonal with respect to the singular function, and for the E_z even modes

$$E_{xm}^b(x) = \frac{\partial E_{zm}^b(x)}{\partial x} = \left[1 - \left(\frac{2x}{a_1}\right)^2\right]^{-1/2} T_{2m+1}\left(\frac{2x}{a_1}\right) \quad (20)$$

for $m = 0, 1, \cdots, N$. For the E_z odd modes, substitute $2m$ for $2m+1$ in the above equation. It should be noted that the series for $\tilde{E}_{zm}^b$ for the E_z odd modes starts from $m = 1$ instead of zero since the zeroth terms of $E_z^b(x)$ is not zero at the fin edges as the boundary condition requires.

V. Results and Discussions

Several configurations will be investigated, and their cross sections are given in Fig. 2. These are referred to as (a) sandwich ferrite-dielectric (SWFD), (b) double layer ferrite-dielectric (DLFD), (c) double layer dielectric-ferrite (DLDF), (d) dual-ferrite (DF), and (e) dual-ferrite-dielectric (DFD) loaded asymmetric finline.

A. Convergence Test

Table I shows the convergence of solutions for $\beta_+/\kappa_0, \beta_-/\kappa_0$ and the differential phase shift $(\beta_+ - \beta_-)/\kappa_0 = \Delta\beta/\kappa_0$ with N in (20) at 30 GHz, for the dominant mode of the SWFD structure. Clearly, good convergence is achieved using small values of N. In fact, $N = 1$ can be used to obtain the solutions of β_+/κ_0 and β_-/κ_0 to four significant digits and $N = 2$ is sufficient to achieve convergence of $\Delta\beta/\kappa_0$ to four significant digits. This fast convergence is attributed not only to the variational nature of the determination of propagation constants using Galerkin's method, but also

TABLE I
CONVERGENCE OF SOLUTIONS FOR $\beta_+/\kappa_0, \beta_-/\kappa_0$ AND $\Delta\beta/\kappa_0$ OF THE DOMINANT MODE OF AN ASYMMETRICAL SANDWICH FERRITE-DIELECTRIC LOADED FINLINE AT THE FREQUENCY OF 30 GHz ON N IN (20) ($\varepsilon_{rf} = \varepsilon_{rd} = 12.5, h_f = h_d = 0.25$ mm, $h_0 = h_1 = 3.306$ mm, $a_0 = 2.1336$ mm, $a = 3.556$ mm, $a_1 = 1.2$ mm, $H_0 = 500$ Oe AND $M_0 = 5000$ Ga)

N	β_+/k_0	β_-/k_0	$(\beta_+ - \beta_-)/k_0$
1	2.36690	2.18964	.17726
2	2.36691	2.18960	.17731
3	2.36690	2.18958	.17732
4	2.36690	2.18956	.17734
5	2.36690	2.18957	.17733
6	2.36688	2.18954	.17734

to the adequate choice of only one set of basis functions. The convergence shown above is typical of that obtained at other frequencies and for the other structures investigated here. The computed data in the rest of this paper has been obtained using $N = 2$.

B. Comparisons with Published Data

The accuracy of our solutions can be assessed by comparison with calculated and measured data available in the literature for particular structures. The first comparison is with computed data obtained by Kitazawa in [6] and by Geshiro and Itoh in [5] for the symmetrical double-layer finlines with a magnetic ferrite. The comparison is shown in Fig. 3 and excellent agreement is apparent.

The particular symmetrical case with a dielectric substrate is also considered. Present results are compared with both the computed results obtained by the transverse resonance diffraction (TRD) method and the measured results as reported by Olley in [14]. This comparison is shown in Fig. 4. Again good agreement is obtained.

C. Single Ferrite Case

It is well known that the single-layer ferrite-loaded planar waveguide structures including symmetrical finlines do not exhibit high nonreciprocity [4]. An additional high permittivity dielectric layer is often introduced to improve nonreciprocal characteristics [3]. We now investigate the differential phase shift and the bandwidth that can be obtained in the SWFD, DLFD, and DLDF structures shown in Fig. 2.

It is known that the useable bandwidth of a phase shifter is limited at low end by the magnetic loss of the ferrite and the lowest frequency of the bandwidth is determined by $f_l = \gamma M_0/0.7$. In this paper M_0 is chosen to be 5000 Ga and therefore $f_l = 20$ GHz. On the other hand, the excitation of the higher-order modes limits the bandwidth at the high end because signal propagation in the higher-order modes can degrade the performance of the phase shifter. Therefore, in a phase shifter with a fixed value of magnetization saturation, a higher cut-off frequency of the first higher-order mode is desirable.

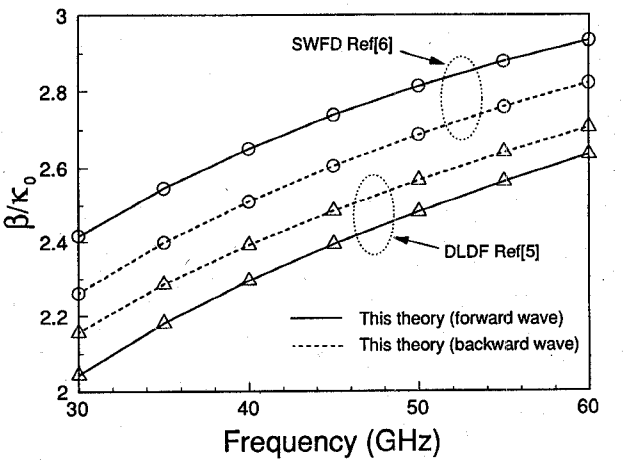

Fig. 3. Comparison of the normalized propagation constants for the dominant mode of symmetrical SWFD and DLDF loaded fin lines with those reported by Kitazawa in [6] and by Geshiro and Itoh in [5] ($\varepsilon_{rf} = \varepsilon_{rd} = 12.5, h_f = h_d = 0.25$ mm, $h_0 = h_1 = 2.1$ mm, $a_0 = a = 2.35$ mm, $a_1 = 1.0$ mm, $H_0 = 500$ Oe, and $M_0 = 5000$ Ga).

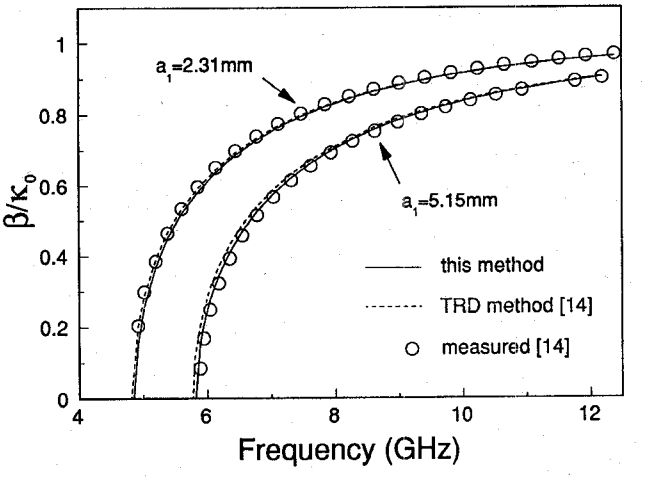

Fig. 4. Comparison of the normalized propagation constants for the dominant mode of symmetrical single-layer dielectric loaded fin lines with computed and measured data [14] ($h_f = 0, \varepsilon_{rd} = 2.2$, $h_d = 0.254$ mm, $h_1 = 11.176$ mm, $a = 10.16$ mm, $h_0 = 11.43$ mm, and $a_0 = 10.16$ mm).

Fig. 5 shows the normalized differential phase shifts of the dominant mode of the three structures as a function of a_0/a. As a_0/a decreases, the asymmetry becomes higher, and the normalized differential phase shift increases for the SWFD and DLFD but decreases for the DLDF. Fig. 6 shows the normalized propagation constants of the backward wave of the dominant and first higher-order modes of the SWFD as a function of a_0/a. Clearly, as the asymmetry increases, the cut-off frequency of the first higher-order mode increases, resulting in an increase in the bandwidth. This behavior is also observed for the DLFD and DLDF. The above results show that the additional design degree of freedom of the asymmetry can be used to enhance the bandwidth and nonreciprocity that can be obtained.

Fig. 7 shows normalized propagation constants of the backward waves of the dominant and first higher-order modes of three double-layer structures as a function of frequency. The

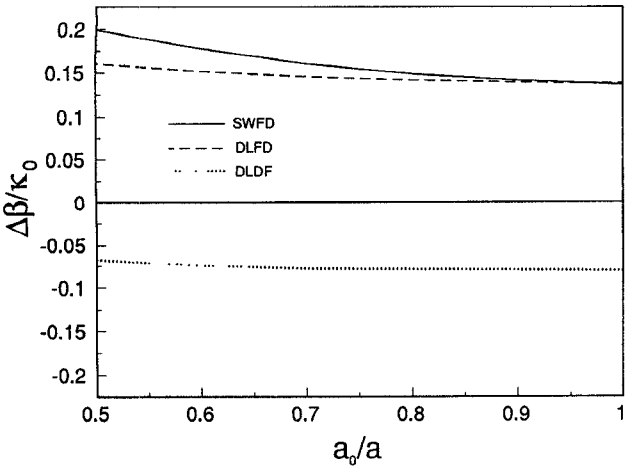

Fig. 5. Normalized differential phase shifts of the dominant mode of the asymmetrical SWFD, DLFD, and DLDF loaded finlines as a function of $a_0/a(\varepsilon_{rf} = \varepsilon_{rd} = 12.5, h_f = h_d = 0.25$ mm, $h_0 = h_1 = 3.306$ mm, $a = 3.556$ mm, $a_1 = 1.2$ mm, $H_0 = 500$ Oe, $M_0 = 5000$ Ga, and $f = 30$ GHz).

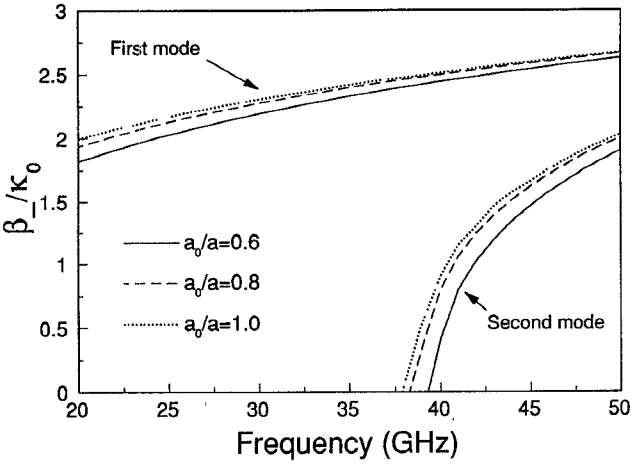

Fig. 6. Normalized propagation constants of the backward waves of the dominant and first higher-order modes of the asymmetrical SWFD loaded finline as a function of frequency for various values of $a_0/a(\varepsilon_{rf} = \varepsilon_{rd} = 12.5, h_f = h_d = 0.25$ mm, $h_0 = h_1 = 3.306$ mm, $a = 3.556$ mm, $a_1 = 1.2$ mm, $H_0 = 500$ Oe, and $M_0 = 5000$ Ga).

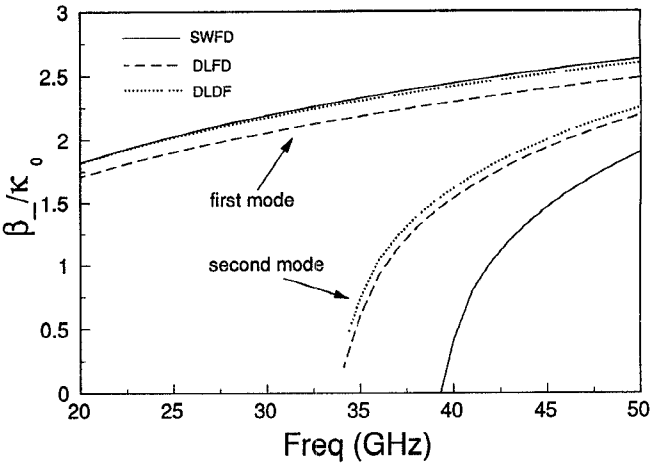

Fig. 7. Normalized propagation constants of the backward waves of the dominant and first higher-order modes of asymmetrical SWFD, DLFD, and DLDF loaded finlines as a function of frequency $(\varepsilon_{rf} = \varepsilon_{rd} = 12.5, h_f = h_d = 0.25$ mm, $h_0 = h_1 = 3.306$ mm, $a_0 = 2.1336$ mm, $a = 3.556$ mm, $a_1 = 1.2$ mm, $H_0 = 500$ Oe, and $M_0 = 5000$ Ga).

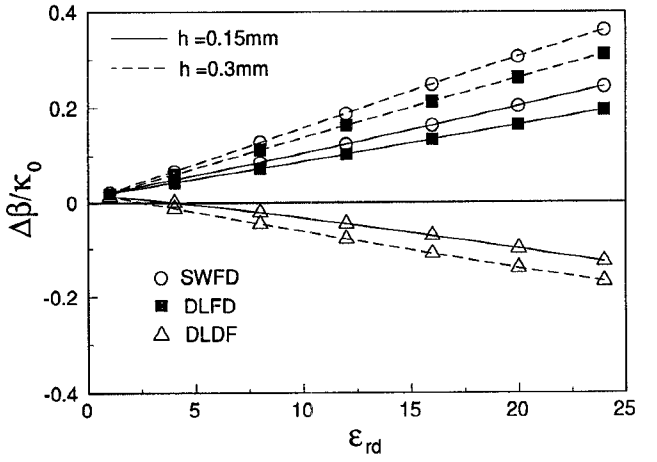

Fig. 8. Normalized differential phase shifts of the dominant mode of the asymmetrical SWFD, DLFD, and DLDF loaded finlines as a function of ε_{rd} for different values of $h_d(\varepsilon_{rf} = 12.5, h_f = 0.25$ mm, $h_f + h_0 = h_d + h_1 = 3.556$ mm, $a_0 = 2.1336$ mm, $a = 3.556$ mm, $a_1 = 1.2$ mm, $H_0 = 500$ Oe, $M_0 = 5000$ Ga, and $f = 30$ GHz).

cut-off frequencies of the first higher-order mode are almost the same for the DLFD and DLDF, but lower by about 5 GHz than that for the SWFD. Therefore, the bandwidth of the SWFD is much wider than that of the other two structures.

Fig. 8 compares the normalized differential phase shifts of the dominant mode for the three structures as a function of ε_{rd} for different values of h_d. For the SWFD and DLFD the differential phase shift is always positive and increases as ε_{rd} and h_d increase. This occurs as the propagation constant for the forward wave increases more quickly with increasing ε_{rd} and h_d than that for the backward wave. This is due to the difference in the field distributions in the dielectric layer of these two counter-propagating waves. On the other hand, for the DLDF the differential phase shift is positive for small values of ε_{rd}, and can be equal to zero at a specific value of ε_{rd}. Beyond this value of ε_{rd} the shift becomes negative and its absolute value increases as ε_{rd} increases. It is also evident that the SWFD offers the highest nonreciprocity in propagation constants.

According to the above results, the SWFD is the best choice among the double-layer single-ferrite loaded structures for realizing good performance phase shifters in terms of nonreciprocity and bandwidth.

D. Dual Ferrite Case

As demonstrated in the previous subsection, the double-layer single-ferrite loaded structure can achieve very high nonreciprocity by using a large value of relative permittivity of the dielectric layer. However, the bandwidth is significantly reduced as overmoding occurs at a lower frequency. The dual ferrite (DF) structure is a structure that may increase nonreciprocity without sacrificing bandwidth. The structure

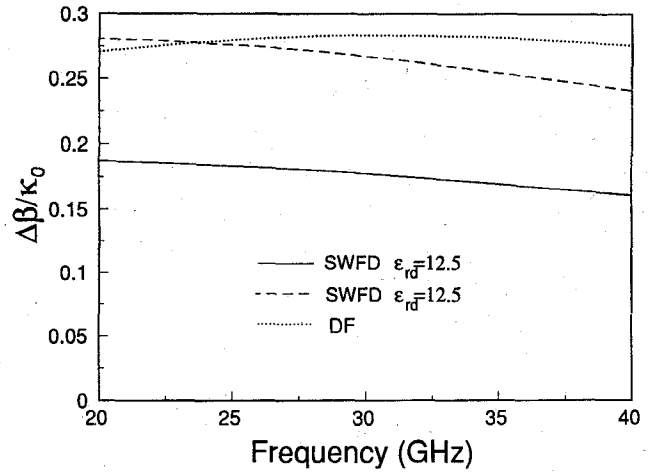

Fig. 9. Normalized differential phase shifts of the dominant mode of the asymmetrical DF and SWFD loaded finlines as a function of frequency ($\varepsilon_{rf} = 12.5, h_f = h_d = 0.25$ mm, $h_0 = h_1 = 3.306$ mm, $a_0 = 2.1336$ mm, $a = 3.556$ mm, $a_1 = 1.2$ mm, $H_0 = 500$ Oe, and $M_0 = 5000$ Ga).

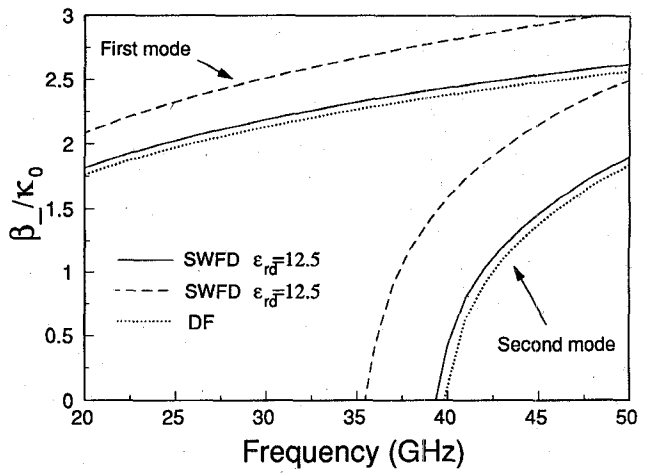

Fig. 10. Normalized propagation constants of backward waves of the dominant and first higher-order modes of the asymmetrical DF and SWFD loaded finlines as a function of frequency ($\varepsilon_{rf} = 12.5, h_f = h_d = 0.25$ mm, $h_0 = h_1 = 3.306$ mm, $a_0 = 2.1336$ mm, $a = 3.556$ mm, $a_1 = 1.2$ mm, $H_0 = 500$ Oe, and $M_0 = 5000$ Ga).

is shown in Fig. 2 and consists of metal fins sandwiched between two ferrites. These ferrites are magnetically saturated in opposite directions. Since the ellipticity of magnetic field is opposite in the two ferrites, nonreciprocity is expected to be much higher than that of the corresponding single-ferrite structure.

Fig. 9 shows the normalized differential phase shifts of the dominant mode of the DF and the SWFD with $\varepsilon_{rd} = 19.0$ as a function of frequency. Fig. 10 shows the normalized propagation constants of the backward wave of the first two modes of these two structures. Both structures have similar nonreciprocity in the frequency range examined. However, the cut-off frequency of the first higher-order mode for the SWFD is lower by about 5 GHz than that for the DF, resulting in a narrower bandwidth for the SWFD. The bandwidth of the SWFD can be made wider by using a smaller value of ε_{rd}. This, however, significantly reduces the nonreciprocity of this structure. This can be clearly seen from the results for the SWFD with $\varepsilon_{rd} = 12.5$, which are also included in Figs. 9 and 10.

In practice, dielectric layers have to be inserted between the two ferrites in the dual-ferrite slotline structure to prevent magnetic leakage from one ferrite to the other [15]. Also, the addition of these thin high permittivity dielectric layers can greatly increase the nonreciprocity. Consequently, we examine the dual-ferrite-dielectric (DFD) finline structure in Fig. 2.

Fig. 11 shows the normalized propagation constants of forward and backward waves of the dominant mode of the DFD, and their differential phase shift, as a function of ε_{rd} for two different values of h_d. In this structure, the electromagnetic field concentrates near the slot (in the dielectric layer) more for the forward wave than for the backward wave. As a result, the propagation constant of the forward wave increases more rapidly than that of the backward wave as ε_{rd} increases, yielding higher nonreciprocity. Such behavior has also been seen in dual-ferrite slotlines [15].

Fig. 12 shows normalized differential phase shifts of the dominant mode of the modified DF as a function of h_d for two

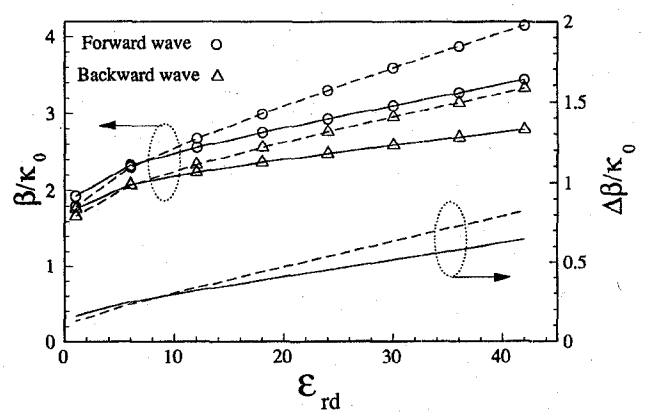

Fig. 11. Normalized propagation constants and phase shift of the dominant modes of the asymmetrical DFD loaded finline as a function of ε_{rd} for $h_d = 0.04$ mm (——) and $h_d = 0.08$ mm (- - - -). ($\varepsilon_{rf} = 12.5, h_f = 0.25$ mm, $h_d + h_0 = h_d + h_1 = 3.306$ mm, $a_0 = 2.1336$ mm, $a = 3.556$ mm, $a_1 = 1.2$ mm, $H_0 = 500$ Oe, $M_0 = 5000$ Ga, and $f = 30$ GHz).

different values of ε_{rd}. The differential phase shift increases very rapidly with h_d when h_d is small. There is an optimum value of h_d for maximum nonreciprocity. This value is quite small, and the bandwidth is only a little less than in the situation when $h_d = 0$.

Fig. 13 shows the normalized differential phase shifts of the dominant mode of the modified DF as a function of a_1. From this figure, we find that when a_1 increases, nonreciprocity increases. Therefore, a relatively wide aperture can be chosen to realize a phase shifter with higher nonreciprocity.

VI. Conclusion

An accurate, extended spectral domain analysis has been presented for the nonreciprocal propagation characteristics of asymmetrical multilayer finlines containing magnetized ferrites. Computed results are in good agreement with calculated and measured data available in the literature. Also,

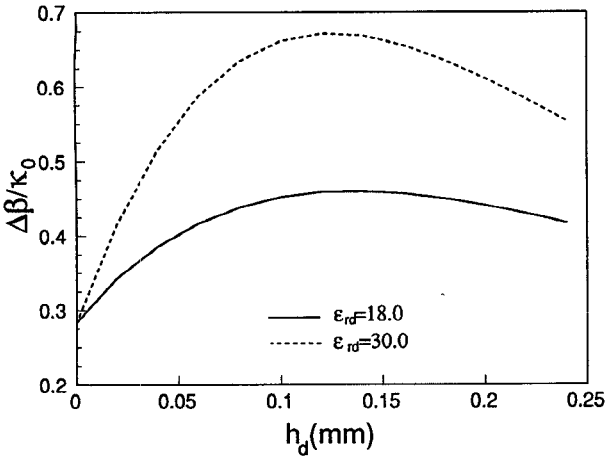

Fig. 12. Normalized differential phase shifts of the dominant mode of the asymmetrical DFD loaded finline as a function of h_d for different values of $\varepsilon_{rd}(\varepsilon_{rf} = 12.5, h_f = 0.25$ mm, $h_d + h_0 = h_d + h_1 = 3.306$ mm, $a_0 = 2.1336$ mm, $a = 3.556$ mm, $a_1 = 1.2$ mm, $H_0 = 500$ Oe, $M_0 = 5000$ Ga, and $f = 30$ GHz).

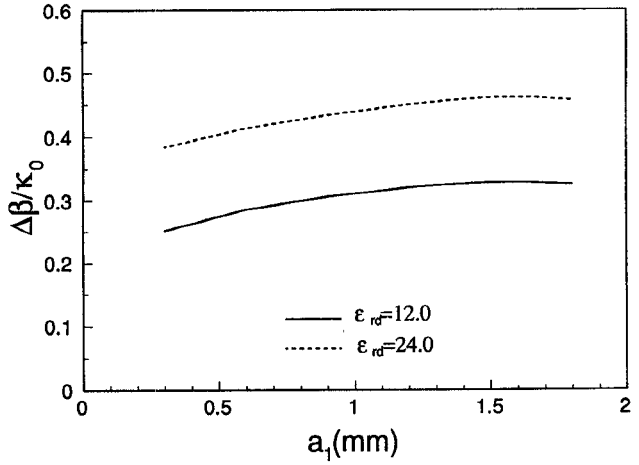

Fig. 13. Normalized differential phase shifts of the dominant mode of the asymmetrical DFD loaded finline as a function of a_1 for different values of $\varepsilon_{rd}(\varepsilon_{rf} = 12.5, h_f = 0.25$ mm, $h_d = 0.04$ mm, $h_0 = h_1 = 3.266$ mm, $a_0 = 2.1336$ mm, $a = 3.556$ mm, $H_0 = 500$ Oe, $M_0 = 5000$ Ga, and $f = 30$ GHz).

the convergence of the solutions for nonreciprocal propagation constants is very good.

The analysis can also be applied to other multilayer planar structures with magnetized ferrites. Compared to the conventional spectral domain approach, the extended method offers several additional features. The method is applicable to planar structures with nonuniform cross-section geometries. The recursive algorithm can be used to efficiently derive the dyadic Green's function for multilayer anisotropic media. Further, only one set of basis functions is needed to calculate the Fourier transforms of the tangential electric field components at the aperture interface.

It has been shown that compared with the conventional finlines, the additional degree of freedom offered by the asymmetry can be used to give higher nonreciprocity, except for the double layer dielectric-ferrite case. Among the two-layer configurations containing a single magnetized ferrite, the sandwich ferrite-dielectric one offers the highest nonreciprocity and the widest bandwidth. By increasing the relative permittivity of the dielectric layer high nonreciprocity can be obtained with single-ferrite structures, however, the bandwidth becomes narrower.

The dual ferrite structure exhibits much higher nonreciprocity without sacrificing the bandwidth compared to the single ferrite structures. Further improvement in nonreciprocity can be achieved by adding thin dielectric layers between the ferrites. An optimum value of the thickness of the dielectric layers for maximum nonreciprocity is apparent. This optimum value is quite small, resulting in only a slight decrease in the bandwidth. Therefore, the four-layer dual-ferrite finline is very suitable for the applications to efficient nonreciprocal phase shifters.

Appendix
Determination of Submatrices in (6)

A. $[P_i]$ and $[R_i]$

For the dielectric layer

$$[P_i] = \frac{1}{\alpha_n^2 + \beta^2}\begin{bmatrix} \beta^2 G_1 - \alpha_n^2 G_2 & -\alpha_n\beta(G_1 + G_2) \\ -\alpha_n\beta(G_1 + G_2) & \alpha_n^2 G_1 - \beta^2 G_2 \end{bmatrix} \tag{21}$$

$$[R_i] = \frac{1}{\alpha_n^2 + \beta^2}\begin{bmatrix} \beta^2 G_3 - \alpha_n^2 G_4 & -\alpha_n\beta(G_3 + G_4) \\ -\alpha_n\beta(G_3 + G_4) & \alpha_n^2 G_3 - \beta^2 G_4 \end{bmatrix} \tag{22}$$

where

$$G_1 = -jr_i/(\omega\mu_0 \tanh r_i h_i), \quad G_3 = G_1/\cosh r_i h_i$$
$$G_2 = -j\omega\varepsilon_0\varepsilon_{ri}/(r_i \tanh r_i h_i), \quad G_4 = G_2/\cosh r_i h_r$$
$$r_i^2 = \alpha_n^2 + \beta^2 - \kappa_0^2\varepsilon_{ri}, \quad \kappa_0^2 = \omega^2\mu_0\varepsilon_0.$$

For the ferrite layer

$$[P_i] = [N_P][W]_2^{-1} \tag{23}$$
$$[R_i] = [N_R][W]_2^{-1} \tag{24}$$

where $[W]_2^{-1}$ is a 4×2 matrix consisting of the last two columns of the inverse of the following matrix $[W]$

$$[W] = \begin{bmatrix} 0 & 1 & 0 & ZB \\ a_{21} & a_{22} & a_{23}B & a_{24}B \\ T_+ & 1 & ZT_- & Z \\ a_{41} & a_{42} & a_{43} & a_{44} \end{bmatrix} \tag{25}$$

$$[N_P] = \begin{bmatrix} a_{31} & a_{32} & a_{33} & a_{34} \\ -YT_+ & -Y & -T_- & -1 \end{bmatrix} \tag{26}$$

$$[N_R] = \frac{1}{P_+}\begin{bmatrix} a_{11} & a_{12} & a_{13}B & a_{14}B \\ 0 & -Y & 0 & -B \end{bmatrix} \tag{27}$$

with

$$a_{11} = C_2\gamma_+ Y + C_4\gamma_+; \quad a_{12} = C_1 Y + C_3$$
$$a_{13} = C_2\gamma_- + C_4\gamma_- Z; \quad a_{14} = C_1 + C_3 Z$$
$$a_{21} = C_6\gamma_+ Y + C_2\gamma_+; \quad a_{22} = C_5 Y + C_1$$
$$a_{23} = C_6\gamma_- + C_2\gamma_- Z; \quad a_{24} = C_5 + C_1 Z$$
$$a_{31} = C_1 Y T_+ + C_2\gamma_+ Y + C_3 T_+ + C_4\gamma_+$$
$$a_{32} = C_1 Y + C_2\gamma_+ Y T_+ + C_3 + C_4\gamma_+ T_+$$
$$a_{33} = C_1 T_- + C_2\gamma_- + C_3 Z T_- + C_4\gamma_- Z$$
$$a_{34} = C_1 + C_2\gamma_- T_- + C_3 Z + C_4\gamma_- Z T_-$$
$$a_{41} = C_5 Y T_+ + C_6\gamma_+ Y + C_1 T_+ + C_2\gamma_+$$
$$a_{42} = C_5 Y + C_6\gamma_+ Y T_+ + C_1 + C_2\gamma_+ T_+$$
$$a_{43} = C_5 T_- + C_6\gamma_- + C_1 Z T_- + C_2\gamma_- Z$$
$$a_{44} = C_5 + C_6\gamma_- T_- + C_1 Z + C_2\gamma_- Z T_-$$
$$C_0 = (\alpha_n^2 - \kappa_i^2\mu_r)^2 - (\kappa_i^2\kappa)^2 \quad C_1 = \alpha_n\beta(\alpha_n^2 - \kappa_i^2\mu_r)/C_0$$
$$C_2 = -\kappa_i^2\kappa\alpha_n/C_0 \quad C_3 = -j\omega\varepsilon_0\varepsilon_{ri}\kappa\beta\kappa_i^2/C_0$$
$$C_4 = j\omega\varepsilon_0\varepsilon_{ri}(\alpha_n^2 - \kappa_i^2\mu_r)/C_0 \quad C_5 = j\omega\mu_0\kappa\beta\alpha_n^2/C_0$$
$$C_6 = -j\omega\mu_0[\mu_r(\alpha_n^2 - \kappa_i^2\mu_r) + \kappa_i^2\kappa^2]/C_0$$
$$B = P_+/\cosh\gamma_- h_i, \quad P_+ = \cosh\gamma_+ h_i$$
$$T_+ = \tanh\gamma_+ h_i, \quad T_- = \tanh\gamma_- h_i$$
$$Z = \eta_e/(\gamma_-^2 - \gamma_e^2) \quad Y = \eta_h/(\gamma_+^2 - \gamma_h^2)$$

B. $[S_i]$ and $[T_i]$

$[S_i]$ and $[T_i]$ can be easily obtained from the expressions of $[R_i]$ and $[P_i]$ by replacing h_i by $-h_i$, respectively.

REFERENCES

[1] L. E. Davis and D. B. Sillars, "Millimetric nonreciprocal coupled-slot finline components," *IEEE Trans. Microwave Theory Tech.*, vol. MTT-34, pp. 804–808, July 1986.

[2] A. Beyer and K. Solbach, "A new fin-line ferrite isolator for integrated millimeter-wave circuits," *IEEE Trans. Microwave Theory Tech.*, vol. MTT-29, pp. 1344–1348, Dec. 1981.

[3] G. Bock, "New multilayered slot line structures with high nonreciprocity," *Elec. Lett.*, vol. 19, pp. 966–968, Nov. 1983.

[4] Y. Hayashi and R. Mittra, "An analytical investigation of finlines with magnetized ferrite substrate," *IEEE Trans. Microwave Theory Tech.*, vol. MTT-31, pp. 495–498, June 1983.

[5] M. Geshiro and T. Itoh, "Analysis of double-layered finlines containing a magnetized ferrite," *IEEE Trans. Microwave Theory Tech.*, vol. MTT-35, pp. 1377–1381, Dec. 1987.

[6] T. Kitazawa, "Analysis of shielded striplines and finlines with finite metallization thickness containing magnetized ferrites" *IEEE Trans. Microwave Theory Tech.*, vol. 39, pp. 70–74, Jan. 1991.

[7] P. Espes *et al.*, "Asymmetrical finline for space applications using millimeter waves," *IEEE Trans. Microwave Theory Tech.*, vol. 37, pp. 289–297, Feb. 1989.

[8] C. H. Chan *et al.*, "A mixed spectral-domain approach for dispersion analysis of suspended planar transmission lines with pedestals," *IEEE Trans. Microwave Theory Tech.*, vol. MTT-37, pp. 1716–1723, Nov. 1989.

[9] L. Schmidt and T. Itoh, "Spectral domain analysis of dominant and higher order modes in fin-lines," *IEEE Trans. Microwave Theory Tech.*, vol. MTT-28, pp. 981–985, Sept. 1980.

[10] T. Itoh, "Spectral domain immitance approach for dispersion characteristics of generalized printed transmission lines," *IEEE Trans. Microwave Theory Tech.*, vol. MTT-28, pp. 733–736, July 1980.

[11] C. M. Krowne, "Determination of the Green's function in the spectral domain using a matrix method: application to radiators or resonators immersed in a complex anisotropic layered medium," *IEEE Trans. Antennas Propagat.*, vol. AP-34, pp. 247–253, Feb. 1986.

[12] F. L. Mesa, R. Marques, and M. Horno, "A general algorithm for computing bidimensional spectral Green's dyad in multilayered complex bianisotropic media: the equivalent boundary method," *IEEE Trans. Microwave Theory Tech.*, vol. 39, pp. 1640–1649, Sept. 1991.

[13] Z. Fan and S. R. Pennock, "Broadside coupled strip inset dielectric guide and its directional coupler application", *IEEE Trans. Microwave Theory Tech.*, vol. 43, pp. 612–619, Mar. 1995.

[14] C. A. Olley, "The characterization of unilateral finline by transverse resonance diffraction," Ph.D. dissertation, Univ. of Bath, U.K., 1987.

[15] E. El-Sharawy and C. J. Koza, "Dual-ferrite slot line for broadband, high nonreciprocity phase shifters," *IEEE Trans. Microwave Theory Tech.*, vol. 39, pp. 2204–2210, Dec. 1991.

Z. Fan received the B.Sc. degree in physics from Hubei University, in 1983, and the M.Sc. degree in microwave and antennas from Wuhan University, P.R. China, in 1986. In 1994, he received the Ph.D. degree from the University of Bath, U.K.

From 1988 to 1991, he was a Lecturer at Wuhan University. Since 1995, he has been a Research Associate at Royal Military College of Canada. His research interests are in the areas of novel waveguide structures, microstrip antennas, dielectric resonator antennas, ferrite devices, and microwave circuits.

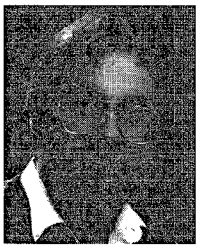

Steve R. Pennock (M'88) was born in Birmingham, U.K., in 1959. He received the B.Sc. degree in physics with electronics from the University of Liverpool, U.K., in 1980, and the Ph.D. degree from the University of Bath, U.K., in 1986 for his work on the plasmatic control of dielectric waveguides.

From 1983 to 1985 he was a Research Assistant working on finline components for millimeter waves at the University of Bath, where, in 1985 he became a Lecturer. His current research interests include the modeling of novel transmission lines, uniform and nonuniform transmission structures, antennas, active and control circuits, and measurements and systems, at microwave and millimeter wave frequencies.